Scaling laws governing the multiple scattering of diatomic molecules under Coulomb explosion

Peter Sigmund
Physics Division, Argonne National Laboratory, Argonne, Illinois 60439
and Physics Department, Odense University, DK-5230 Odense M, Denmark*
(Received 27 April 1992)

The trajectories of fast molecules during and after penetration through foils are governed by Coulomb explosion and distorted by multiple scattering and other penetration phenomena. A scattering event may cause the energy available for Coulomb explosion to increase or decrease, and angular momentum may be transferred to the molecule. Because of continuing Coulomb explosion inside and outside the target foil, the transmission pattern recorded at a detector far away from the target is not just a linear superposition of Coulomb explosion and multiple scattering. The velocity distribution of an initially monochromatic and well-collimated, but randomly oriented, beam of molecular ions is governed by a generalization of the standard Bothe-Landau integral that governs the multiple scattering of atomic ions. Emphasis has been laid on the distribution in relative velocity and, in particular, relative energy. The statistical distributions governing the longitudinal motion (i.e., the relative motion along the molecular axis) and the rotational motion can be scaled into standard multiple-scattering distributions of atomic ions. The two scaling laws are very different. For thin target foils, the significance of rotational energy transfer is enhanced by an order of magnitude compared to switched-off Coulomb explosion. A distribution for the total relative energy (i.e., longitudinal plus rotational motion) has also been found, but its scaling behavior is more complex. Explicit examples given for all three distributions refer to power-law scattering. As a first approximation, scattering events undergone by the two atoms in the molecule were assumed uncorrelated. A separate section has been devoted to an estimate of the effect of impact-parameter correlation on the multiple scattering of penetrating molecules. That effect is by and large unrelated to Coulomb explosion, but some attention is indicated since it is an unavoidable feature in all scattering phenomena involving molecular ions.

PACS number(s): 34.40.+n, 34.50.Ez, 34.20.Gj

I. INTRODUCTION

Experiments with molecular-ion beams penetrating solids at energies in the upper-keV and MeV range may provide rich information but also present considerable challenges in the interpretation [1]. The interest in such experiments was stimulated originally by the discovery that diatomic molecules can be transmitted intact through foils of thicknesses exceeding the mean free path for dissociation by several orders of magnitude [2]. A systematic effort went into probing wake fields of penetrating ions via the mutual interaction between the atoms in a molecule [3,4]. More recently, interest turned to determining molecular structures by detecting the fragments of dissociated molecules in coincidence [5]. In the past few years, a considerable potential has shown up to image the internal nuclear motion of small molecular ions in high-resolution coincidence experiments [6].

Coulomb explosion is a central feature in all penetration phenomena involving swift molecular ions. Transmission patterns, i.e., recorded distributions in energy loss and scattering angle of diatomic molecules after penetration through thin foils, show a characteristic ring structure as a result of Coulomb explosion [7]. This effect governs the motion of the fragments during penetration through the material and, notably, in the vacuum between the target and the detection device. It has become evident gradually that observable effects of the medium on molecule penetration, such as those of wake forces, stopping, and multiple scattering, get strongly distorted by Coulomb explosion [8–13].

A recent study of the dynamics of diatomic molecules under Coulomb explosion [12] showed that the effect of a force acting on a molecule parallel to its axis is heavily suppressed in the Coulomb image. Conversely, the effect of a torque is always enhanced. Thus, strong anisotropies must be expected to affect the Coulomb images of all common penetration phenomena. Little general knowledge is available about the magnitude of these effects, and qualitative insight is blurred by geometrical complications: There are two natural frames of reference, one related to the beam and another one to the molecular axis. Scattering events are best described in terms of beam-oriented coordinates, but the dynamics of a Coulomb-exploding molecule emerges most readily in a frame of reference aligned with the molecular axis. That axis is oriented at random in typical experiments.

A theoretical scheme for a comprehensive treatment was outlined in Ref. [12]. That treatment was based on the assumption that Coulomb explosion dominates, and that all other ongoing processes act as small perturbations. That assumption is amply justified in many molecular-ion experiments, as can be seen, e.g., by inspection of a measured ring pattern [1,7]. A relationship was established between the velocity changes experienced by a molecule during penetration and the ultimate velocity

change recorded at a detector far away from the penetrated foil. That transformation is linear but depends on the orientation and configuration of the molecule. The treatment covered the dynamics comprehensively but was only very sketchy with regard to the statistics of collision events.

The present study is a follow-up on the statistical aspects of the problem. The aim has been to establish scaling laws that relate statistical distributions governing molecules under Coulomb explosion to the corresponding distributions with the Coulomb explosion switched off. A numerical simulation of the effect of multiple scattering on Coulomb-exploding molecules for a particular system has been published recently [14].

The scaling laws derived in this paper become useful in practice provided that multiple-scattering distributions for molecules that are unaffected by Coulomb explosion are available. As a first approximation, those may be constructed by convoluting distributions of independently scattered atomic fragments [9–11,13–14]. However, at least for molecules approximately aligned with the beam, impact parameters and hence scattering angles must be more or less correlated. That effect has been discussed in a slightly different context [15], but information on the overall importance of impact-parameter correlation appears unavailable. At least a qualitative estimate is needed.

II. RECAPITULATION

This section serves to summarize and supplement the main results on the dynamics of Coulomb-exploding molecules reported in Ref. [12]. Consider a diatomic molecule with atomic masses M_A, M_B. The atoms A and B move initially with a laboratory velocity $\mathbf{v}_0$ and are separated by a vector distance $\mathbf{D}$. At time $t=0$, the molecule is thought to enter a material medium (gaseous or solid) and to be rapidly stripped of a number of electrons. The molecule will dissociate, and thereafter the two fragments will repel each other via their mutual Coulomb force. If the internal motion of the molecule in its initial state could be neglected, and if nothing else were happening, their relative speed v_∞ would be determined by

$$\frac{M_0}{2}v_\infty^2=\frac{q_A q_B}{D}\ , \tag{1}$$

where M_0 is the reduced mass and q_A and q_B are ionic charges. The quantity v_∞ will be called the unperturbed Coulomb speed.

The action of the medium on the penetrating molecule is assumed to come in small increments in the velocities $\mathbf{v}_A, \mathbf{v}_B$ of the two atoms. Such changes in velocity are caused by elastic and inelastic collisions or perhaps by the action of an electric field over a small time interval. Let one of these velocity increments occur at some specified time t (≥ 0) and let it lead to a change in relative velocity,

$$\Delta\mathbf{v}=\Delta\mathbf{v}_A-\Delta\mathbf{v}_B\ . \tag{2}$$

Most often, molecular fragments are not recorded *in situ* but far away from the target. Then, the recorded relative velocity is *not* the vector sum of $\Delta\mathbf{v}$ and the unperturbed Coulomb velocity $\mathbf{v}_\infty$. Indeed, take first $\Delta\mathbf{v}$ parallel to the molecular axis. Let the relative speed at time $t=\infty$ be $v(\infty)$, and let $v(t)$ be the relative speed at the time of the event. Energy is conserved in the time intervals $(0,t)$ and (t,∞), whereas a jump occurs at time t. This yields

$$v(\infty)=[v_\infty^2+2v(t)\Delta v+\Delta v^2]^{1/2}\ . \tag{3}$$

Only increments Δv much smaller than v_∞ will be of interest throughout this paper. Therefore, Eq. (3) may be linearized to

$$v(\infty)=v_\infty+\Delta v(\infty)\ , \tag{4}$$

with $\Delta v(\infty)=[v(t)/v_\infty]\Delta v$.

The relative speed v at time t may be expressed by the Coulomb-exploded distance $r=r(t)$. In terms of this variable, $\Delta v(\infty)$ reduces to

$$\Delta v(\infty)=P(r/D)\Delta v\ , \tag{5}$$

with

$$P(r/D)=(1-D/r)^{1/2} \tag{6}$$

for unscreened Coulomb interaction. For straight superposition of Coulomb explosion and multiple scattering, one would have expected that $P\equiv 1$. Figure 1 shows that P is always less than 1 and approaches zero for r approaching D, i.e., t approaching 0. For $t=0$, the quadratic term in Eq. (3) prevents $\Delta v(\infty)$ from going literally to zero. However, the conclusion prevails that a kick given to a molecule *parallel* to its axis in the initial stage of Coulomb explosion will not significantly affect the relative motion asymptotically. On this basis, it was concluded in Ref. [12] that the vibrational motion of a molecule

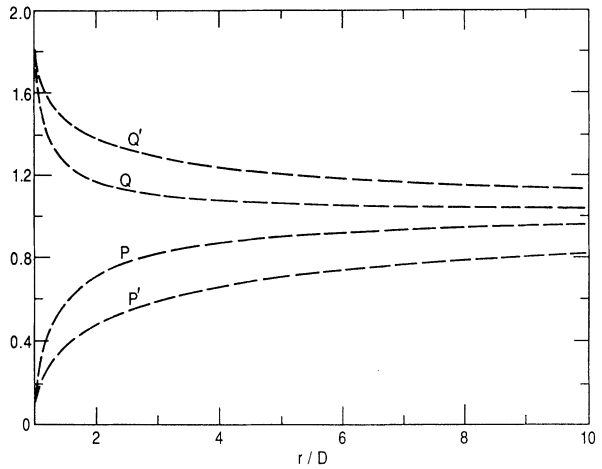

FIG. 1. Factors P and Q governing the Coulomb image $\Delta\mathbf{v}(\infty)$ of a velocity increment $\Delta\mathbf{v}$ according to Eqs. (5) and (6) and (9) and (10). D is the initial internuclear distance of the impinging molecule, and $r=r(t)$ is the internuclear distance at the time of the event that gives rise to the velocity increment. Also shown is an effective value P' as defined by Eq. (18), and the corresponding quantity Q'. For those two curves, $r=r(\tau)$ is the internuclear distance at the exit from the foil. Thin-foil experiments typically cover the range of $r/D\lesssim 1$. A graph showing that regime on a bigger scale may be found in Ref. [12].

in its initial state may safely be neglected as a factor distorting the Coulomb image. The same does not necessarily apply to the rotational motion. Moreover, even though the vibrational *velocity* may be ignored, the fact that the internuclear *distance* D is distributed in accordance with the vibrational state of the incident molecule is crucial and needs to be allowed for.

An analogous consideration, based on angular momentum conservation, was applied in Ref. [12] to determine the effect of a kick perpendicular to the molecular axis. Such a kick will get the molecule to rotate, but while angular momentum is conserved, the moment of inertia increases gradually due to Coulomb explosion. Therefore, the angular velocity will decrease, and the angle of rotation will approach some asymptotic value. The Coulomb explosion will be unaffected by rotational motion up to first order in Δv since it is governed by energy conservation. Altogether, this results in an angle of rotation given by

$$\phi(\infty)=r(t)\Delta v\int_t^\infty \frac{dt'}{r(t')^2} , \tag{7}$$

where $r(t')$ is governed by the differential equation for unperturbed Coulomb explosion,

$$dr'/dt=v_\infty(1-D/r')^{1/2} . \tag{8}$$

After integration of (7) one finds

$$\Delta v(\infty)=v_\infty\phi(\infty)=Q(r/D)\Delta v , \tag{9}$$

with

$$Q(r/D)=2(r/D)[1-(1-D/r)^{1/2}] . \tag{10}$$

As in Eq. (5), the time dependence has been expressed in terms of the Coulomb-exploded distance $r=r(t)$. Figure 1 shows that the dependence of Q on r/D is opposite to that of P. Indeed, Q is always greater than 1, i.e., Coulomb explosion *enhances* the effect of a lateral kick. The reason for this behavior is obvious: The Coulomb velocity follows the rotation of the molecular axis and hence receives a component perpendicular to the initial axis.

Consider now a small velocity increment $\Delta\mathbf{v}$ in an arbitrary direction. In view of the linear dependence of Eqs. (5) and (9) on Δv, its effect can be split into components parallel and perpendicular to the axis. Hence,

$$\Delta\mathbf{v}(\infty)=P(\Delta\mathbf{v}\cdot\boldsymbol{\Omega})\boldsymbol{\Omega}+Q[\Delta\mathbf{v}-(\Delta\mathbf{v}\cdot\boldsymbol{\Omega})\boldsymbol{\Omega}] , \tag{11}$$

where

$$\boldsymbol{\Omega}=\mathbf{D}/D \tag{12}$$

is a unit vector parallel to the molecular axis. Equation (11) can be cast into a more compact form,

$$\Delta\mathbf{v}(\infty)=\mathsf{T}(r)\cdot\Delta\mathbf{v} , \tag{13}$$

where T is a tensor with the elements

$$T_{ij}=Q\delta_{ij}+(P-Q)\Omega_i\Omega_j \quad \text{for } i,j=1,2,3 . \tag{14}$$

In the absence of Coulomb explosion, one has $P=Q=1$, and T reduces to the unit matrix. This identity transformation applies to the change $\Delta\mathbf{V}$ in the center-of-mass velocity which is unaffected by Coulomb explosion.

Superposition of the effects caused by a sequence of events, each governed by Eq. (13) and happening at times t_ν leads to a total change in relative velocity,

$$\Delta\mathbf{v}(\infty)=\sum_\nu \mathsf{T}(t_\nu)\cdot\Delta\mathbf{v}_\nu=\sum_\nu \mathsf{T}(r_\nu/D)\cdot\Delta\mathbf{v}_\nu . \tag{15}$$

For continuous action, (15) leads to

$$\Delta\mathbf{v}(\infty)=\int_0^\tau dt\,\mathsf{T}(t)\cdot[\mathbf{F}_A(t)/M_A-\mathbf{F}_B(t)/M_B] , \tag{16}$$

where $\mathbf{F}_A$ and $\mathbf{F}_B$ are forces on A and B, respectively, and τ is the time interval during which these forces are acting, i.e., typically the dwell time in a foil.

If the forces are independent of time, Eq. (16) takes on the particularly appealing form

$$\Delta\mathbf{v}(\infty)=\tau\mathsf{T}'\cdot(\mathbf{F}_A/M_A-\mathbf{F}_B/M_B) , \tag{17}$$

where T' is a matrix of the same form as (14), but with $P(t)$ and $Q(t)$ replaced by

$$P'=\frac{1}{\tau}\int_0^\tau P(t)dt=\frac{\int_D^{r(\tau)}dr(1-D/r)^{-1/2}P(r/D)}{\int_D^{r(\tau)}dr(1-D/r)^{1/2}} , \tag{18}$$

and correspondingly for Q'. These effective P' and Q' values are also shown in Fig. 1. They are relevant whenever the effective force, be it deterministic or stochastic, does not vary significantly across the target. Note how slowly these functions approach the asymptotic behavior.

III. STATISTICS

For collision-induced events, Eq. (15) remains valid, but both the total number of events and their time sequence are distributed stochastically. Therefore, Eqs. (16) and (17) can only be satisfied in the average. The distribution in the accumulated velocity change can be constructed if the probabilities for individual events are given as functions of time. For collision events, those probabilities are governed by the pertinent cross sections. The statistical description of particle penetration has been reviewed in a recent series of lectures [16]. Only a few central results and input assumptions will be mentioned here.

For simplicity, consider first the center-of-mass motion which is only indirectly affected by Coulomb explosion. The distribution in the center-of-mass velocity $\mathbf{V}$ of scattered molecules is given by the Bothe-Landau integral

$$F(\mathbf{V})=\frac{1}{(2\pi)^3}\int d^3k\, e^{i\mathbf{k}\cdot(\mathbf{V}-\mathbf{v}_0)} \times\exp\left[-Nv_0\int_0^\tau dt\,\sigma_V(\mathbf{k},t)\right] , \tag{19}$$

with the transport cross section

$$\sigma_V(\mathbf{k},t)=\int d\sigma(\Delta\mathbf{V},t)(1-e^{-i\mathbf{k}\cdot\Delta\mathbf{V}}) . \tag{20}$$

Here $\mathbf{v}_0$ is the initial beam velocity, $d\sigma(\Delta\mathbf{V},t)$ the differential cross section, and N the number density of scattering centers. $Nv_0dt\,d\sigma(\Delta\mathbf{V},t)$ is the probability for a collision event leading to an increment in center-of-

mass velocity $(\Delta\mathbf{V}, d(\Delta\mathbf{V}))$ in the time interval (t, dt). $F(\mathbf{V})$ is normalized to 1 and reduces to a Dirac function when there are no collisions. Equation (19) is valid under the assumption of statistical independence of the individual collision events. In addition, it is assumed that the total change in beam velocity is so small that any variation of the cross section with speed can be neglected. However, a dependence of the cross section on time has been allowed for since the molecular geometry undergoes changes due to ongoing Coulomb explosion.

Equation (19) is three dimensional: The Landau integral for the energy-loss spectrum emerges by integration over the lateral velocity, and vice versa for the Bothe integral that governs the angular distribution.

Consider now the corresponding relations for the relative motion. In the absence of collisions, we have

$$\mathbf{v} - v_\infty \boldsymbol{\Omega} - \mathbf{v}_d = 0 \ , \tag{21}$$

where $\mathbf{v}$ is the relative velocity at the detector position, $v_\infty \boldsymbol{\Omega}$ the unperturbed Coulomb velocity, and $\mathbf{v}_d$ any other deterministic velocity change expressed by Eq. (16). The initial internal motion of the molecule may be included in this term too: Even though that velocity is statistically distributed, the pertinent average is independent of what happens during penetration and can hence be carried out separately.

When collisions are allowed for, the left-hand side of Eq. (21) will be distributed around zero and governed by the transport cross section

$$\sigma_v(\mathbf{k}, t) = \int d\sigma(\Delta\mathbf{v}, t)(1 - e^{-i\mathbf{k}\cdot\mathsf{T}(t)\cdot\Delta\mathbf{v}}) \ , \tag{22}$$

Equation (22) differs from (20) by the appearance of the matrix T in the exponent. This originates in the fact that we are looking for a change in the observable velocity at $t = \infty$, [cf. Eq. (15)]. The matrix does not enter the argument of $d\sigma$ since the cross section determines the statistics of the velocity change *at the time of the event.*

With this, the distribution in relative velocity $\mathbf{v}$ reads

$$F(\mathbf{v}) = \frac{1}{(2\pi)^3} \int d^3k \, e^{i\mathbf{k}\cdot(\mathbf{v} - \mathbf{v}_c)} \times \exp\left[-N v_0 \int_0^\tau dt \, \sigma_v(\mathbf{k}, t) \right] \ , \tag{23}$$

where

$$\mathbf{v}_c = v_\infty \boldsymbol{\Omega} + \mathbf{v}_d \ . \tag{24}$$

The joint distribution of $\mathbf{v}$ and $\mathbf{V}$ could be found by the same argument but will not be discussed explicitly. For completeness, the distribution in laboratory velocity $\mathbf{v}_A$ of just one of the atoms in the molecule will be mentioned since it refers to an experimentally important quantity [1]. From

$$\mathbf{v}_A = \mathbf{V} + \frac{M_B}{M}\mathbf{v} \ , \tag{25}$$

one readily finds

$$F(\mathbf{v}_A) = \frac{1}{(2\pi)^3} \int d^3k \, e^{i\mathbf{k}\cdot[\mathbf{v}_A - \mathbf{v}_0 - (M_B/M)\mathbf{v}_c]} \times \exp\left[-N v_0 \int_0^\tau dt \, \sigma\left[\mathbf{k}, \frac{M_B}{M}\mathbf{k}, t \right] \right] \ , \tag{26}$$

where

$$\sigma(\mathbf{K}, \mathbf{k}, t) = \int d\sigma(\Delta\mathbf{V}, \Delta\mathbf{v}, t)(1 - e^{-i\mathbf{K}\cdot\Delta\mathbf{V} - i\mathbf{k}\cdot\mathsf{T}(t)\cdot\Delta\mathbf{v}}) \ . \tag{27}$$

The following approximation will prove very useful:

$$\int_0^\tau dt \, \sigma(P(t), Q(t), \cdots) \simeq \tau\sigma(P', Q', \cdots) \ . \tag{28}$$

Here, σ indicates any of the transport cross sections considered above, and P' and Q' are the quantities introduced in and after Eq. (18), respectively. Equation (28) is inspired by Eq. (18), which was exact for a constant force. Equation (28) is very accurate in the limit of thin foils where $Q(t)$ varies only slowly with t and where $P(t)$ is unimportant in comparison with $Q(t)$. The relation is also valid in the limit of very thick foils when P and Q approach 1. Minor errors may be expected at intermediate thicknesses.

As they stand, all distributions refer to a fixed initial orientation $\boldsymbol{\Omega}$ of the penetrating molecule as well as a given internuclear distance D.

IV. CROSS SECTIONS

Further evaluation requires a closer look at the transport cross sections. For swift, dissociated molecules, we may operate with individual scattering events between the atoms of the molecule and the constituents of the target. For the soft interactions that are of interest in this context, this implies that the outcome of a collision between one atom of the molecule and a target atom is independent of whether or not the other atom collides with the same target atom. This, however, does not preclude some geometric correlation through correlated impact parameters. The latter must be allowed for, at least for molecules well aligned with the beam (Fig. 2).

Differential cross sections are conveniently expressed in terms of the velocity increments $\Delta\mathbf{v}_A, \Delta\mathbf{v}_B$ experienced by the individual atoms. By addition and subtraction of appropriate terms, Eq. (27) can be recast in the form

$$\sigma(\mathbf{K}, \mathbf{k}, t) = \sigma_A\left[\frac{M_A}{M}\mathbf{K} + \mathbf{k}\cdot\mathsf{T} \right] + \sigma_B\left[\frac{M_B}{M}\mathbf{K} - \mathbf{k}\cdot\mathsf{T} \right] - \Delta\sigma_{AB}(\mathbf{K}, \mathbf{k}, t) \ , \tag{29}$$

where

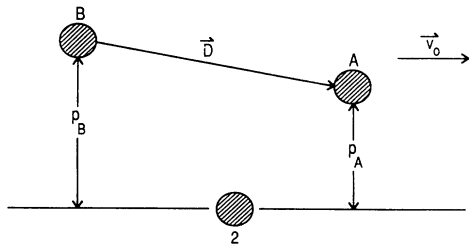

FIG. 2. Impact-parameter-correlated scattering: 2 is a target atom, A and B are atoms making up a diatomic molecule moving with velocity $\mathbf{v}_0$, and p_A and p_B are impact parameters (Sec. VII).

$$\sigma_A(k)=\int d\sigma(\Delta\mathbf{v}_A)(1-e^{-i\mathbf{k}\cdot\Delta\mathbf{v}_A}) \tag{30}$$

and correspondingly for $\sigma_B(k)$. Moreover,

$$\Delta\sigma_{AB}(\mathbf{K},\mathbf{k},t)=\int d\sigma(\Delta\mathbf{v}_A,\Delta\mathbf{v}_B,t)(1-e^{-i[(M_A/M)\cdot\mathbf{K}+\mathbf{k}\cdot\mathsf{T}]\cdot\Delta\mathbf{v}_A})\times(1-e^{-i[(M_B/M)\cdot\mathbf{K}-\mathbf{k}\cdot\mathsf{T}]\cdot\Delta\mathbf{v}_B}) . \tag{31}$$

The transport cross sections $\sigma_A(k)$ and $\sigma_B(k)$ refer to penetrating atomic ions and thus do not depend on time. $\Delta\sigma_{AB}$ accounts for the correlation between the scattering events undergone by atoms A and B. A similar decomposition proved useful in the theory of the penetration of atomic projectiles through molecular *targets* [17,18].

With (31), Eqs. (20) and (22) reduce to

$$\sigma_V(\mathbf{k},t)=\sigma_A\left[\frac{M_A}{M}\mathbf{k}\right]+\sigma_B\left[\frac{M_B}{M}\mathbf{k}\right]-\Delta\sigma_{AB}(\mathbf{k},0,t) \tag{32}$$

and

$$\sigma_v(\mathbf{k},t)=\sigma_A(\mathbf{k}\cdot\mathsf{T})+\sigma_B(-\mathbf{k}\cdot\mathsf{T})-\Delta\sigma_{AB}(0,\mathbf{k},t) . \tag{33}$$

The correlation term will initially be neglected. An estimate of its significance will be given in Sec. VII.

For swift ions, momentum is exchanged between the projectile atoms and the target via screened-Coulomb scattering on the target nuclei and via electronic stopping. Electronic stopping changes the velocity component along the beam direction, while screened-Coulomb scattering affects the lateral velocity component. It is of interest to estimate the magnitudes of the respective contributions to the momentum transfer. In either case, it is the *fluctuation* that is of interest.

Consider first the component parallel to the beam. The pertinent quantity in penetration theory is the energy-loss straggling $\langle\Delta E^2\rangle$. It is related to the fluctuation in the beam velocity v_b by

$$\langle\Delta v_b^2\rangle=\frac{\langle\Delta E^2\rangle}{M_1^2v_0^2}\simeq\frac{4\pi Nv_0\tau Z_1^2Z_2^2e^4}{M_1^2v_0^2} , \tag{34}$$

where Bohr's value [16,19] has been inserted for the straggling. The index 1 denotes a projectile atom A or B, and 2 a target atom. The Z_i are atomic numbers, and e denotes the elementary charge.

The velocity component v_p perpendicular to the beam may be estimated from multiple-scattering theory [16,19]:

$$\langle\Delta v_p^2\rangle=v_0^2\langle\alpha^2\rangle\simeq\frac{4\pi Nv_0\tau Z_1^2Z_2^2e^4}{M_1^2v_0^2}L_n , \tag{35}$$

where α denotes the laboratory scattering angle and $L_n\simeq\ln(T_{\max}/T_{\min})$. Here, $T_{\max}$ and $T_{\min}$ are effective bounds on the energy transfer in screened-Coulomb collisions with the target nuclei.

From (34) and (35) one finds a ratio

$$\frac{\langle\Delta v_b^2\rangle}{\langle\Delta v_p^2\rangle}\simeq\frac{1}{Z_2L_n} . \tag{36}$$

For ions of several MeV/u, the quantity L_n is typically of the order of 20. Even for low-Z_2 targets, the ratio (36) lies far enough below 1 to make energy-loss straggling a small perturbation in comparison with multiple scattering. Note that the ratio (36) depends only weakly on the beam velocity except through the logarithm.

At this point it may be appropriate to pay attention to the initial rotational motion of the molecule compared to the rotational motion induced by multiple scattering. In a small-angle elastic-scattering event, the projectile scattering angle ψ and the energy transferred to a target atom 2 are related by $\Delta E=(M_1/M_2)\psi^2E_0$, where $E_0=M_1v_0^2/2$ is the energy of a beam atom (A or B). With an angular resolution of 1 mrad, a beam energy of 1 MeV, and a mass ratio $M_1/M_2=1$, ΔE becomes 1 eV, which is three orders of magnitude above typical rotational energies. Hence, rotational zero-point motion is a very minor disturbance for this set of parameters. It may become more important in experiments with much higher resolution at lower beam energies, but only under drastically different circumstances will it be dominating.

V. RELATIVE MOTION

The distribution in relative velocity $\mathbf{v}$ is determined by Eqs. (23) and (33). In the following, the approximation (28) will be applied. This sets an upper limit to the foil thickness such that $r/D\lesssim 1$ and implies that most of the Coulomb explosion takes place outside the target. This is the standard situation in Coulomb imaging [5,6]. Figure 1 shows that this is also the regime in which deviations from "normal" dynamics are most pronounced.

Then, Eq. (23) reads

$$F(\mathbf{v})=\frac{1}{(2\pi)^3}\int d^3k\, e^{i\mathbf{k}\cdot(\mathbf{v}-\mathbf{v}_c)}\exp[-Nv_0\tau\sigma(\mathbf{k}\cdot\mathsf{T}')] , \tag{37}$$

with

$$\sigma(\mathbf{k})=\sigma_A(\mathbf{k})+\sigma_B(-\mathbf{k}) , \tag{38}$$

insofar as impact-parameter correlations are negligible.

Equation (37) suggests introduction of a new integration variable [12],

$$\mathbf{K}=\mathbf{k}\cdot T' , \tag{39}$$

by means of which Eq. (37) reduces to

$$F(\mathbf{v})=\frac{1}{P'Q'^2}F_0[(\mathsf{T}')^{-1}\cdot(\mathbf{v}-\mathbf{v}_c)] , \tag{40}$$

with

$$F_0(\mathbf{v})=\frac{1}{(2\pi)^3}\int d^3k\, e^{i\mathbf{k}\cdot\mathbf{v}}\exp[-Nv_0\tau\sigma(\mathbf{k})] . \tag{41}$$

The inverse tensor has the form

$$(\mathsf{T}')^{-1}=\frac{1}{Q'}\delta_{ij}+\left[\frac{1}{P'}-\frac{1}{Q'}\right]\Omega_i\Omega_j , \tag{42}$$

as is easily verified by multiplication with (14).

In view of Eq. (38), the distribution (41) has the sym-

metry properties of a multiple-scattering distribution for atomic projectiles. On the basis of the estimates presented in the end of Sec. IV, we may ignore energy-loss straggling and write F_0 in the form

$$F_0(\mathbf{v})=\delta(v_x)f_0(\mathbf{v}_\rho) . \tag{43}$$

Here, the x axis has been chosen along the beam, and $\mathbf{v}_\rho$ denotes the component of $\mathbf{v}$ perpendicular to the beam. The function

$$f_0(\mathbf{v}_\rho)=\frac{1}{(2\pi)^2}\int d^2\kappa\, e^{i\boldsymbol{\kappa}\cdot\mathbf{v}_\rho}\exp[-Nv_0\tau\sigma(\kappa)] \tag{44}$$

is a two-dimensional multiple-scattering distribution with cylindrical symmetry, i.e., $f_0(\mathbf{v}_\rho)\equiv f_0(v_\rho)$. Apart from a scaling factor, this is the type of distribution analyzed in Ref. [20], with v_ρ related to the scattering angle α by $v_\rho=v_0\alpha$ for small angles.

Consider first the distribution in longitudinal velocity, $v_\Omega=(\mathbf{v}\cdot\boldsymbol{\Omega})$, i.e., the relative motion parallel to the molecular axis. Take into account only Coulomb explosion and multiple scattering, i.e., set $v_d=0$ in Eq. (24) since the initial rotation is negligible. Then, we have

$$F(v_\Omega)=\int d^3v\,\delta[v_\Omega-(\mathbf{v}\cdot\boldsymbol{\Omega})]F(\mathbf{v}) \tag{45}$$

and

$$(\mathsf{T}')^{-1}\cdot(\mathbf{v}-\mathbf{v}_c)=\frac{\mathbf{v}}{Q'}+\left[\frac{1}{P'}-\frac{1}{Q'}\right](\boldsymbol{\Omega}\cdot\mathbf{v})\boldsymbol{\Omega}-\frac{v_\infty}{P'}\boldsymbol{\Omega} . \tag{46}$$

After integration over the angular part of $\mathbf{v}$ by use of spherical coordinates, one finds

$$F(v_\Omega)=\frac{2}{P'Q'^2}\int v\,dv \times f_0\left[\left[\frac{v^2-v_\Omega^2}{Q'^2}+\frac{(v_\Omega-v_\infty)^2}{P'^2}\right]^{1/2}\right] \times\left[\frac{(v^2-v_\Omega^2)}{Q'^2}\sin^2\theta-\frac{(v_\Omega-v_\infty)^2}{P'^2}\cos^2\theta\right]^{-1/2} , \tag{47}$$

where θ is the angle between the molecular axis and the beam direction. The bounds on the integral over v are determined by the requirement that both square roots be real.

Equation (47) demonstrates the obvious fact that a molecule aligned with the beam ($\theta=0$) cannot pick up a longitudinal velocity component v_Ω by multiple scattering. Equation (47) needs in general to be averaged over $\cos\theta$, i.e., over all orientations of the molecular axis. For a uniform distribution, one finds

$$F(v_\Omega)=\frac{\pi}{P'Q'^2}\int v\,dv\frac{f_0\left[\left[\frac{v^2-v_\Omega^2}{Q'^2}+\frac{(v_\Omega-v_\infty)^2}{P'^2}\right]^{1/2}\right]}{\left[\frac{v^2-v_\Omega^2}{Q'^2}+\frac{(v_\Omega-v_\infty)^2}{P'^2}\right]^{1/2}} . \tag{48}$$

The square root may be introduced as the integration variable. With this, Eq. (48) reduces to the appealing form

$$F(v_\Omega)=\frac{\pi}{P'}\int_{|v_\Omega-v_\infty|/P'}^{\infty}dv' f_0(v') . \tag{49}$$

Equation (49) is a scaling law relating the multiple-scattering distribution including Coulomb explosion to a distribution of uncharged pairs of atoms. Note that f_0 is normalized according to

$$\int_0^\infty 2\pi v'dv' f_0(v')=1 . \tag{50}$$

Consider next the distribution in rotational energy,

$$E_{\rm rot}=\frac{M_0}{2}(v^2-v_\Omega^2) . \tag{51}$$

In view of the occurrence of v_Ω in (51), it is possible to start the evaluation from Eq. (48). After introduction of suitable variables and integration, one finds

$$F(E_{\rm rot})=\frac{2\pi}{Q'^2M_0}\int_{(2E_{\rm rot}/Q'^2M_0)^{1/2}}^{\infty}dv'\frac{f_0(v')}{(v'^2-2E_{\rm rot}/Q'^2M_0)^{1/2}} . \tag{52}$$

Finally, the distribution in total internal energy, $E=M_0v^2/2$, can likewise be found starting from Eq. (48) and reads

$$F(E)=\frac{\pi}{M_0}\int\frac{f_0(v')dv'}{[Q'^2v_\infty^2-(Q'^2-P'^2)(v^2-Q'^2v'^2)]^{1/2}} . \tag{53}$$

The limits on the integration over dv' are given as follows. Introduce parameters v_a, v_1, and v_2 by

$$v_a=\frac{v_\infty Q'^2}{Q'^2-P'^2} , \quad v_1=\frac{|v-v_\infty|}{P'} , \quad v_2=\frac{v+v_\infty}{P'} . \tag{54}$$

For $v<v_a$, v' is bounded by $v_1<v'<v_2$, while for $v>v_a$, the integral in (53) stands for

$$\left[\int_{v_{\rm min}}^{v_2}+\int_{v_{\rm min}}^{v_1}\right]dv' , \tag{55}$$

with

$$v_{\rm min}=\left[\frac{v^2}{Q'^2}-\frac{v_\infty^2}{Q'^2-P'^2}\right]^{1/2} . \tag{56}$$

Note that the distribution (53) cannot be found just by convolution of (52) with the energy distribution corresponding to (49), since (49) and (52) have been averaged *separately* over all orientations of the projectile molecule.

The task remains to scale the unperturbed molecular distribution f_0 as defined by (44) and (38) into the corresponding distributions for atomic ions. Note first that for small-angle multiple scattering, elastic-scattering cross sections may be well approximated by power laws [19]. Then, the transport cross section for an atomic ion reduces to [20]

$$\sigma_0(\kappa)=C'a^2\left[\frac{2Z_1Z_2e^2}{Ea}\right]^{2m}\kappa^{2m}\ , \tag{57}$$

where a is the screening radius characterizing the interaction potential, E the energy, and m an exponent characterizing the screened Coulomb interaction ($0\le m\le 1$). The effective value of m varies slowly with target thickness as well as the atomic numbers and masses of the collision partners [19–21]. The parameter C' is independent of the elements involved. Hence, except for very heteronuclear molecules, the molecular cross section will take on the form of a scaled atomic cross section,

$$\sigma(k)=\sigma_A(\beta\kappa)\ , \tag{58}$$

with

$$\beta=\left[1+\left[\frac{a_B}{a_A}\right]^2\left[\frac{Z_B}{Z_A}\frac{M_A}{M_B}\frac{a_A}{a_B}\right]^{2m}\right]^{1/2m}\ . \tag{59}$$

From Eq. (58) one finds

$$f_0(v')=\frac{1}{(\beta v_0)^2}f_A\left[\frac{v'}{\beta v_0}\right]\ , \tag{60}$$

where $f_A(\alpha)$ is the tabulated multiple-scattering profile for A atoms as a function of scattering angle α [20] and v_0 the beam velocity.

From (52) and (60) one obtains the dimensionless energy variable

$$\varepsilon_{\rm rot}=\frac{2E_{\rm rot}}{M_0(\beta v_0)^2}=\left[\frac{v_{\rm rot}}{\beta v_0}\right]^2 \tag{61}$$

and hence the scaling relation

$$F_{\rm rot}(E)dE=g_{\rm rot}(\varepsilon)d\varepsilon =\frac{\pi\,d\varepsilon}{Q'^2}\int_{\sqrt{\varepsilon/Q'}}^{\infty}d\alpha\frac{f_A(\alpha)}{(\alpha^2-\varepsilon/Q'^2)^{1/2}}\ , \tag{62}$$

and similarly for the longitudinal distribution (49),

$$F_{\rm long}(E)dE=g_{\rm long}(\varepsilon)d\varepsilon =\frac{\pi\,d\varepsilon}{2P'\sqrt{\varepsilon_\infty}}\int_{|\varepsilon-\varepsilon_\infty|/(2P'\sqrt{\varepsilon_\infty})}^{\infty}d\alpha\,f_A(\alpha)\ , \tag{63}$$

where

$$\varepsilon_\infty=(v_\infty/\beta v_0)^2\ . \tag{64}$$

In the transition from longitudinal velocity to longitudinal energy, only first-order terms were kept, in accordance with the step leading from Eq. (3) to Eq. (4).

The corresponding relation for the total internal energy reads

$$g_{\rm tot}(\varepsilon)d\varepsilon=\frac{\pi\,d\varepsilon}{2Q'(Q'^2-P'^2)^{1/2}}\int\frac{f_A(\alpha)d\alpha}{[\alpha^2-(\varepsilon-\varepsilon_a)/Q'^2]^{1/2}}\ , \tag{65}$$

with the bounds following from Eqs. (54) and (56),

$$\begin{aligned}\alpha_1&=\frac{1}{P'}|\sqrt{\varepsilon}-\sqrt{\varepsilon_\infty}|\ ,\\ \alpha_2&=\frac{1}{P'}(\sqrt{\varepsilon}+\sqrt{\varepsilon_\infty})\ ,\\ \alpha_{\rm min}&=\frac{1}{Q'}[\varepsilon-\varepsilon_a]^{1/2}\ .\end{aligned} \tag{66}$$

Equations (62)–(65) make the scaling very explicit: α is the scattering angle in the laboratory system and $f_A(\alpha)$ could be a *measured* multiple-scattering profile for an atomic ion A at the beam velocity v_0 and the target thickness $v_0\tau$. However, theoretical multiple-scattering profiles reported in Ref. [20] are known to agree well with measured profiles in solid and gaseous target materials. Their scaling properties in terms of mass, atomic number, target thickness, and beam energy have been tested thoroughly.

VI. EXAMPLE: POWER-LAW SCATTERING

The familiar picture of a Gaussian multiple-scattering profile is rarely applicable to molecule penetration. For the thin targets utilized frequently, a better approximation is a simple analytic formula that originates in the scattering on a powerlike interaction potential $\propto R^{-2}$ between colliding atoms [22], which can be written in the form [20]

$$f_A(\alpha)=\frac{\alpha_0}{2\pi}\frac{1}{(\alpha^2+\alpha_0^2)^{3/2}}\ , \tag{67}$$

with

$$\alpha_0=\frac{4\pi\lambda a_A Z_A Z_2 e^2 N\tau}{M_A v_0} \tag{68}$$

and $\lambda=0.327$. More important than Eq. (68) in the present context is the fact that $\alpha_0=1.305\alpha_{1/2}$, where $\alpha_{1/2}$ is the half-angle (in radians) for multiple scattering of atom A. Then, the longitudinal spectrum, Eq. (63), reads

$$g_{\rm long}(\varepsilon) =\frac{1}{4P'\alpha_0\sqrt{\varepsilon_\infty}}\left\{1-\left[1+\left[\frac{2P'\alpha_0\sqrt{\varepsilon_\infty}}{\varepsilon-\varepsilon_\infty}\right]^2\right]^{-1/2}\right\}\ . \tag{69}$$

This relation is shown in Fig. 3. Note that (69) represents a Dirac function for $P'=0$.

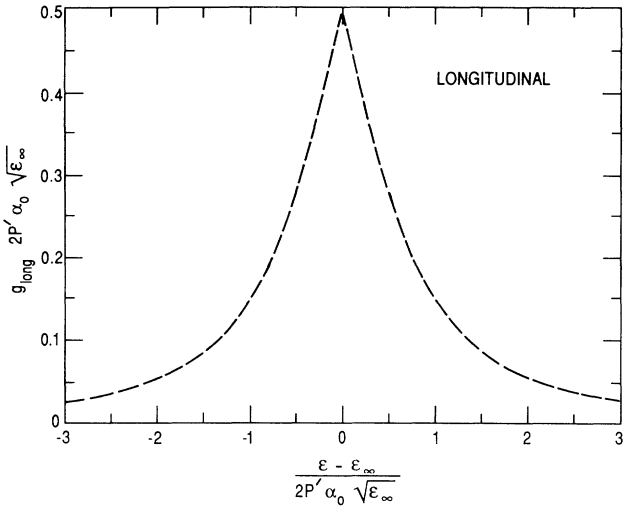

FIG. 3. Distribution of internal energy of a molecule at the detector. Component in the direction of the molecular axis only, Eq. (69). The quantity ε is a dimensionless energy variable, $\varepsilon=2E/(M_0\beta^2 v_0^2)$, and ε_∞ reflects the unperturbed Coulomb energy. The angle α_0 is, apart from a numerical factor, the half-width of the angular multiple-scattering profile of one of the atoms, β a scaling factor converting an atomic into a molecular multiple-scattering profile [cf. Eq. (59)], and v_0 the beam velocity. This curve was evaluated for the $m=\frac{1}{2}$ scattering law [Eq. (67)].

The rotational spectrum, Eq. (62), can be written in the form

$$g_{\rm rot}(\varepsilon)=\frac{1}{2Q'^2\alpha_0^2}\int_0^\infty d\xi\left[1+(\varepsilon/Q'^2\alpha_0^2)\cosh^2\xi\right]^{-3/2} \tag{70}$$

and has been integrated numerically. This relation has been plotted in Fig. 4. At large ε, (70) approaches the asymptotic behavior

$$g_{\rm rot}(\varepsilon)\sim\frac{0.392\alpha_0 Q'}{\varepsilon^{3/2}}\ , \tag{71}$$

which is characteristic of the single-scattering limit.

Finally, the spectrum (65) reads

$$g_{\rm tot}(\varepsilon)d\varepsilon=\frac{d\varepsilon}{4\alpha_0 Q'(Q'^2-P'^2)^{1/2}}\times\int\frac{dt}{(t^2+1)^{3/2}[t^2-(\varepsilon-\varepsilon_a)/Q'^2\alpha_0^2]^{1/2}}\ , \tag{72}$$

with the bounds specified by (66). Here, the integrand depends on the scaled energy variable characterizing the rotational distribution (70), but that simple scaling property is lost due to the bounds on the integral, Eq. (66), which reflect the scaling of the longitudinal spectrum (69). Therefore, this spectrum cannot be expressed by one universal curve. An example is shown in Fig. 5.

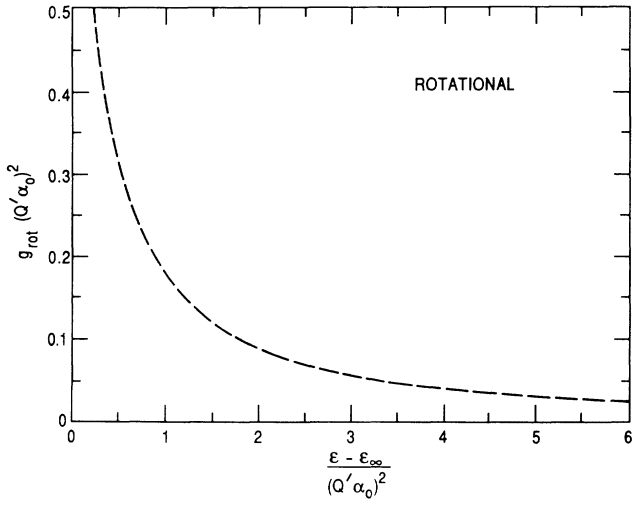

FIG. 4. Distribution of internal energy of a molecule at the detector. Component perpendicular to the direction of the molecular axis only, Eq. (70). Notation as in Fig. 3.

VII. CORRELATED MULTIPLE SCATTERING

It has been demonstrated experimentally and theoretically that correlations in impact parameter affect the multiple-scattering profiles of atomic ions penetrating thin molecular targets [17,23]. Similar effects must be observable for molecular ions penetrating atomic targets. Qualitative estimates may be based upon considering the range of impact parameters that governs the multiple-scattering distribution in a given experimental situation. The thinner the target, the smaller the representative scattering angles, and, hence, the larger the representative impact parameters. Impact-parameter correlations are most pronounced for distant collisions because of the slow variation of the momentum transfer with impact parameter in that limit [15–18].

A comprehensive estimate on the basis of Eqs. (23) and (33) is a major task on its own. The estimate to be given here will be based on the variance

$$\langle\Delta v^2\rangle=Nv_0\tau\int d\sigma(\Delta\mathbf{v}_A-\Delta\mathbf{v}_B)^2\ . \tag{73}$$

In terms of vectorial impact parameters $\mathbf{p}_A,\mathbf{p}_B$ (Fig. 1),

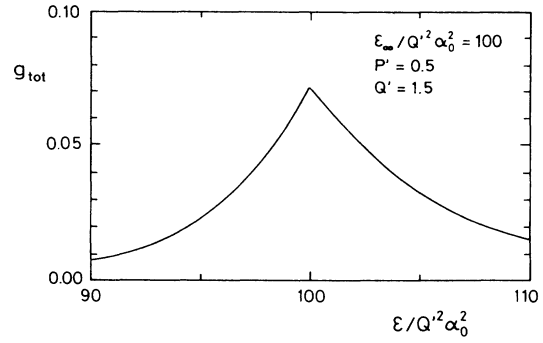

FIG. 5. Distribution of internal energy (longitudinal plus rotational) of a molecule at the detector. Notations as in Fig. 3. As explained in the text, this distribution is not a convolution of two curves of the type shown in Figs. 3 and 4.

the velocity increments imparted to atoms A and B read

$$\Delta\mathbf{v}_A=(\mathbf{p}_A/p_A)\Delta v_A(p_A),\quad \Delta\mathbf{v}_B=(\mathbf{p}_B/p_B)\Delta v_B(p_B)\ , \tag{74}$$

provided that the individual scattering events undergone by projectile atoms exhibit cylindrical symmetry. Impact-parameter correlations can be expressed in terms of a double-differential cross section [16–18],

$$d\sigma=d^2p_A d^2p_B\delta(\mathbf{p}_A-\mathbf{p}_B-\mathbf{b})\ , \tag{75}$$

where $\mathbf{b}$ is the projection of the molecular axis on the impact plane perpendicular to the beam.

Consider the unique case of a homonuclear molecule where, for perfect alignment parallel to the beam, the expression (73) must vanish. For power-law scattering,

$$\Delta v_A(p)=\frac{C_A}{p^s}\ , \tag{76}$$

the integrals containing Δv_A^2 and Δv_B^2 in (73) need to be truncated at some lower limit p^* according to some maximum allowed scattering angle. The precise definition of that angle is immaterial to what follows.

The cross term in Eq. (73) can be evaluated in Fourier space by means of Eqs. (74) and (75). After carrying out the angular integrations, one finds

$$\int d\sigma\,\Delta\mathbf{v}_A\cdot\Delta\mathbf{v}_B=2\pi\int_0^\infty\kappa\,d\kappa\,J_0(\kappa b)\times\int_{p^*}^\infty p_A dp_A\Delta v_A(p_A)J_1(\kappa p_A)\times\int_{p^*}^\infty p_B dp_B\Delta v_B(p_B)J_1(\kappa p_B)\ , \tag{77}$$

where J_0 and J_1 are Bessel functions.

After insertion of (77) into (73) and integration of the square terms, one finds

$$\langle\Delta v^2\rangle=Nv_0 d\tau\frac{\pi C_A^2}{(s-1)p^{*2-2s}}\left[1-2(s-1)\left[\frac{p^*}{b}\right]^{2s-2}\int_0^\infty du\,u^{2s-3}J_0(u)\left[\int_{up^*/b}^\infty dt\,t^{1-s}J_1(t)\right]^2\right]\ . \tag{78}$$

The integrations can be carried out analytically if p^* is set equal to zero within the square brackets. This is justified within the range of convergence of the integrals, which happens to be $1<s<7/4$. Even though this does not include the case $s=2$ considered in Sec. VI, the result is worth considering:

$$\langle\Delta v^2\rangle=Nv_0\tau\frac{\pi C_A^2}{(s-1)p^{*2-2s}}\times\left[1-\left[\frac{p^*}{b}\right]^{2s-2}\frac{\Gamma(s)[\Gamma(\frac{3}{2}-s/2)]^2}{\Gamma(2-s)[\Gamma(\frac{1}{2}+s/2)]^2}\right]\ . \tag{79}$$

This quantity depends on the orientation through

$$b=r(t)\sin\theta\ , \tag{80}$$

where $r=r(t)$ is the internuclear distance at the time of the scattering event.

In view of the slight inconsistency in the above truncation procedure, Eq. (79) becomes invalid for small values of $b<p^*$, i.e., for molecules aligned with the beam. In that limit, Taylor expansion of Eqs. (73)–(75) in powers of b is straightforward [15]. The leading term reads

$$\langle\Delta v^2\rangle=\pi\frac{s^2+1}{2s}Nv_0\tau C_A^2\frac{b^2}{p^{*2s}}\ . \tag{81}$$

Both (79) and (81) imply that multiple scattering is strongly correlated for $\theta\lesssim\theta_0$, with

$$\sin\theta_0\simeq p^*/r(t)\simeq p^*/D\ . \tag{82}$$

For high-energy particles, p^* will typically be of the order of the screening radius of the atomic interaction. Then, only a small fraction of the impinging molecules undergoes correlated multiple scattering. The estimate does not give an indication of which portion of a multiple-scattering profile is affected by impact-parameter correlation. Evidently, such an estimate cannot emerge from consideration of the variance alone.

VIII. DISCUSSION

In the absence of multiple scattering as well as zero-point motion, the distribution of internal energy of a Coulomb-exploded molecule has a sharp peak at the unperturbed Coulomb energy. Figures 3 and 4 demonstrate the effect of collisions, experienced during transmission through a thin foil, on the internal energy spectrum recorded far away from the target foil. The two graphs illustrate separately the effects of collisions leading to longitudinal and rotational energy transfer, respectively. While the longitudinal spectrum is symmetric, the rotational spectrum is nonvanishing only for positive energy transfers and has a sharp edge at $\varepsilon=0$ This difference stems from the different way scattering events affect the dominating Coulomb explosion: Angular momentum transfer is equivalent with a velocity component perpendicular to the axis. The energy associated with it will be positive and proportional to the square of the velocity increment. Conversely, a kick along the axis can either increase or diminish the Coulomb energy, and the change will be linear in the velocity increment.

The widths $\Delta\varepsilon$ of the two distributions are related to the width $\Delta\alpha$ of the angular distribution. For a purely rotational spectrum, Eq. (62) shows that

$$\Delta\varepsilon_{\rm rot}\simeq Q'^2\Delta\alpha^2\ , \tag{83}$$

apart from a numerical factor $\simeq 1$, the accurate value of which depends on the detailed shape of the distribution f_0. Similarly, for a purely longitudinal spectrum, Eq. (63) shows that

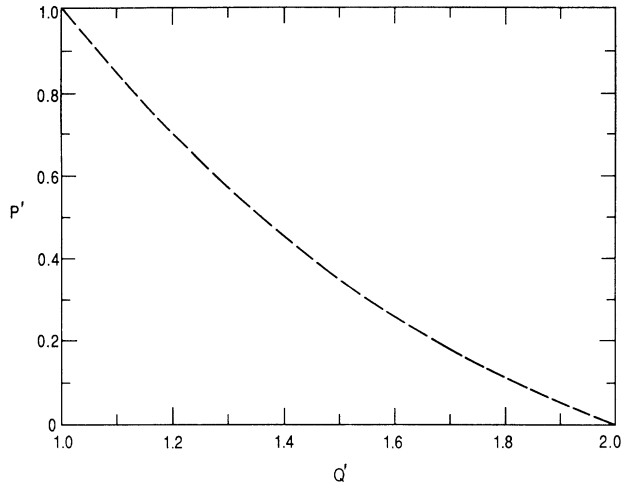

FIG. 6. Related values of P' and Q' extracted from the data underlying Fig. 1.

$$\Delta\varepsilon_{\text{long}} \propto 2P'\alpha_0\sqrt{\varepsilon_\infty} , \tag{84}$$

and the ratio is

$$\frac{\Delta\varepsilon_{\text{rot}}}{\Delta\varepsilon_{\text{long}}} \simeq \frac{Q'^2}{P'}\frac{\beta\alpha_0 v_0}{2v_\infty} . \tag{85}$$

Consider first the "normal" case $P'=Q'=1$. For homonuclear molecules, Eq. (59) leads to $\beta=2$ for $m=\frac{1}{2}$. Then, Eq. (85) reduces to the ratio between the multiple-scattering width $v_0\alpha_0$ in the absence of Coulomb explosion and the unperturbed Coulomb speed v_∞. This is, roughly, the ratio between the width and the radius of a ring pattern, a quantity that is $\ll 1$ in experiments on thin targets where a clear ring pattern is visible. Thus, for $P'=Q'=1$, longitudinal energy transfer dominates.

This behavior changes dramatically when realistic values are inserted for P' and Q'. Figure 6 is a convenient plot to show values of P' and Q' that belong together, and Fig. 7 shows the factor $\delta=P'/Q'^2$, the reciprocal of which enters Eq. (85), as a function of r/D. In the range where $r/D \lesssim 2$, the presence of this factor in Eq. (85) increases the ratio of the half-widths by more than an order of magnitude. Thus, a significant fraction of the energy transferred to the molecule by scattering events goes into purely rotational motion. According to Fig. 4, that part of the spectrum is asymmetric. Unless there is a significant anharmonic component in the vibrational state of an impinging molecule, any skewness in the internal-energy spectrum must be ascribed to rotational energy transfer. The schematic example shown in Fig. 5 (with $P'=0.5$ and $Q'=1.5$) is on the conservative side. Measured as well as simulated spectra reported in Ref. [14] indeed show a high degree of skewness.

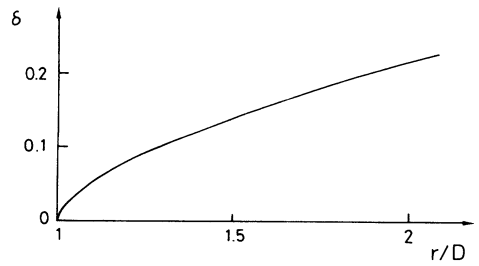

FIG. 7. The factor $\delta=P'/Q'^2$ that enters the ratio between the scaled energy variables [Eq. (82)].

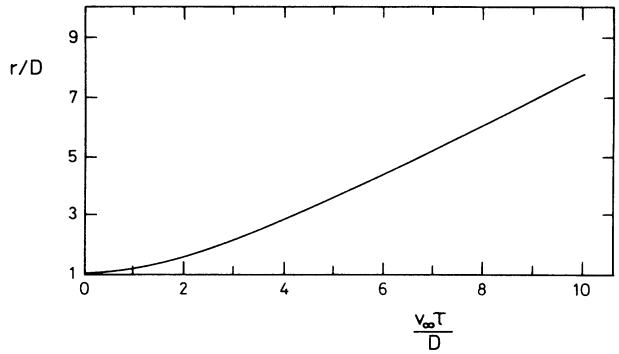

FIG. 8. Universal relation between dwell time τ and Coulomb-exploded distance $r(\tau)$. The quantity v_∞ is the unperturbed Coulomb speed and D the initial internuclear distance.

Figure 8 shows a universal curve for the conversion of Coulomb-exploded distance into target thickness or dwell time. From this, one may construct the dependence of δ on τ, which is shown in Fig. 9. This dependence is seen to be very close to linear in the thickness range corresponding to $r/D \lesssim 2$. Since α_0 goes as the $1/2m$th power of τ [20], one concludes that the ratio (85) goes as $\propto \tau^{1/2m-1}$. For $m=0.5$, it becomes independent of τ.

For thin targets, m can become smaller than 0.5. When that thickness range is accessible, the ratio (85) will go through a minimum at some thickness and then increases when the thickness decreases further. From the results of Ref. [21], one concludes that the turning point should come at $\pi(a_A^2+a_B^2)Nv_0\tau \sim 1$, the accurate number depending on the interatomic potential. This thickness range is reached in Coulomb imaging experiments with target foils with thicknesses below 100 Å.

While the rotational energy is an important ingredient in the half width, a comparison of Eqs. (69) and (70) shows that it must even become dominant in the far tails: For $m=\frac{1}{2}$, the rotational spectrum goes as $\varepsilon^{-3/2}$ accord-

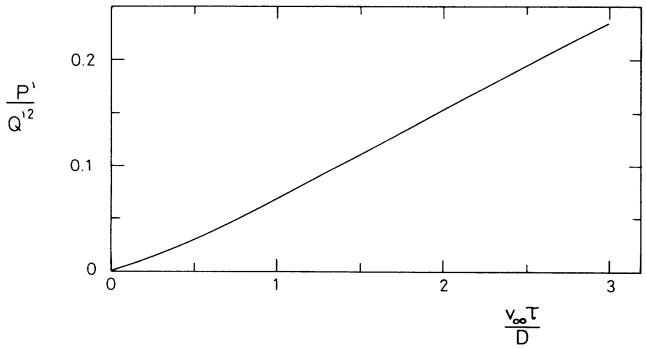

FIG. 9. The factor $\delta=P'/Q'^2$ vs dwell time τ.

ing to Eq. (71), while the longitudinal spectrum goes as $(\varepsilon-\varepsilon_\infty)^{-2}$.

The rotational motion of a Coulomb-exploded molecule is not of much interest in itself, but it broadens the energy profile and thus diminishes the resolution in Coulomb imaging. It appears difficult to separate the rotational motion experimentally since all rotational velocities have become very small by the time the molecule arrives at the detector. Therefore, deconvolution on the basis of calculated spectra, like those reported here or those simulated [14], appears to be the most feasible procedure at this point.

ACKNOWLEDGMENTS

Discussions with D. S. Gemmell, E. P. Kanter, Z. Vager, and, in particular, D. Zajfman are gratefully acknowledged. This work was supported by the U.S. Department of Energy, Office of Basic Energy Sciences, under Contract No. W-31-109-ENG-38, and by the Danish Natural Science Research Council (SNF).

*Address for correspondence.

[1] D. S. Gemmell, Nucl. Instrum. Methods **194**, 255 (1982).
[2] J. C. Poizat and J. Remillieux, J. Phys. B **5**, 94 (1972).
[3] W. Brandt, A. Ratkowski, and R. H. Ritchie, Phys. Rev. Lett. **33**, 1325 (1974); **35**, 130 (1975).
[4] Z. Vager and D. S. Gemmell, Phys. Rev. Lett. **37**, 1352 (1976).
[5] M. J. Gaillard, D. S. Gemmell, G. Goldring, I. Levine, W. J. Pietsch, J. C. Poizat, A. J. Ratkowski, J. Remillieux, Z. Vager, and B. J. Zabransky, Phys. Rev. A **17**, 1797 (1978).
[6] Z. Vager, R. Naaman, and E. P. Kanter, Science **244**, 426 (1989).
[7] J. Golovchenko and E. Lægsgaard, Phys. Rev. A **9**, 1215 (1974).
[8] Yu. Kagan, Yu. V. Kononets, and N. K. Jamankyzov, Zh. Eksp. Teor. Fiz. **74**, 288 (1978); [Sov. Phys.—JETP **47**, 148 (1978)].
[9] R. M. Schectman and W. D. Ruden, Phys. Rev. A **24**, 1327 (1981); Nucl. Instrum. Methods **194**, 295 (1982).
[10] I. Plesser, Nucl. Instrum. Methods **194**, 269 (1982).
[11] D. Zajfman, G. Both, E. P. Kanter, and Z. Vager, Phys. Rev. A **41**, 2482 (1990).
[12] P. Sigmund, Nucl. Instrum. Methods B **67**, 11 (1992).
[13] D. Zajfman, Phys. Rev. A **42**, 5374 (1990).
[14] D. Zajfman, T. J. Graber, E. P. Kanter, and Z. Vager, Phys. Rev. A **46**, 194 (1992).
[15] Yu. V. Kononets and N. K. Jamankyzov, Nucl. Instrum. Methods B **2**, 46 (1984).
[16] P. Sigmund, *in Interaction of Charged Particles with Solids and Surfaces,* Vol. 271 of *NATO Advanced Study Institute,* edited by A. Gras-Marti *et al.* (Plenum, New York, 1991), p. 73.
[17] P. Sigmund, Mat. Fys. Medd. Dan. Vid. Selsk. **39** (11), 1 (1977).
[18] P. Sigmund, Phys. Rev. A **14**, 996 (1976).
[19] N. Bohr, Mat. Fys. Medd. Dan. Vid. Selsk. **18** (8), 1 (1948).
[20] P. Sigmund and K. B. Winterbon, Nucl. Instrum. Methods **119**, 541 (1974); **125**, 491 (1975).
[21] A. D. Marwick and P. Sigmund, Nucl. Instrum. Methods **126**, 317 (1975).
[22] J. Lindhard and V. Nielsen, Mat. Fys. Medd. Dan. Vid. Selsk. **38** (9), 1 (1971).
[23] G. Sidenus, N. Andersen, P. Sigmund, J. Heinemeier, P. Hvelplund, and H. Knudsen, Nucl. Instrum. Methods **134**, 597 (1976).